IEEE Access
Multidisciplinary | Rapid Review | Open Access Journal

Received 22 October 2023, accepted 3 December 2023, date of publication 14 December 2023,
date of current version 4 January 2024.

Digital Object Identifier 10.1109/ACCESS.2023.3342919

RESEARCH ARTICLE

Considerations for Thrust Coefficient Constraints on Axial Induction-Based Optimization

MFON O. CHARLES[1], (Member, IEEE), DAVID T. O. OYEDOKUN[1], (Senior Member, IEEE), AND MQHELE E. DLODLO[2], (Life Member, IEEE)

[1]Department of Electrical Engineering, University of Cape Town, Cape Town 7700, South Africa
[2]National University of Science and Technology (NUST), Bulawayo, Zimbabwe

Corresponding author: Mfon O. Charles (chrmfo001@myuct.ac.za)

This work was supported in part by the Petroleum Development Trust Fund (PTDF), Nigeria; and in part by the Tertiary Education Trust Fund (TETFund) through the University of Calabar, Nigeria.

ABSTRACT Pitching turbine blades into the wind increases the thrust coefficient, C_T, which increases the power generated by the wind turbine. However, excessive C_T increments beyond rotor mean wind speed C_T-equivalent, tend to cause overexertion and increased loads. Consequently, the rated operational lifetime of the turbine is reduced. This study uses a high-fidelity 2-D Gaussian wake model and an augmented version of Frandsen's turbulence intensity (TI) model to simulate a hexagonally deployed wind plant (WP) operation. Turbines' axial-induction factor α is optimised using Particle Swarm Optimisation (PSO) and Genetic Algorithm (GA), to maximise WP power and annual energy production (AEP), with constrains on individual turbine C_T values to remain within rotor wind speed equivalent based on turbine's thrust curve. At a $5D$ minimum turbine-to-turbine (T-2-T) separation distance, results show that C_T constraints on individual turbines increased the wind speed range of healthy operations by up to 66.67% considering extreme loads. AEP gains reduced from 11.91% and 13.25% (optimised without constraints), to approximately 7.59% and 5.74% (with constraints), when compared to the corresponding $5D$ Base case (non-optimised and unconstrained), using PSO and GA, respectively. The study also shows that WP power maximisation can increase turbulence intensity levels within the WP especially if turbines are tightly deployed. The outcome of this study has implications for new wind farm layouts and wind plant power optimization.

INDEX TERMS Annual energy production, wind plant, axial induction factor, power maximisation, thrust coefficient constrain, turbulence intensity, genetic algorithm, particle swarm optimisation.

I. INTRODUCTION

The wind plant (WP) optimization problem is multi-dimensional and has many interacting factors, which cannot be captured entirely as optimization variables. Given a wind power plant site, optimizing or intuitively selecting the best turbine layout at the pre-operation stage and optimizing for improved WP power while reducing turbine loads in the operational stage is often sufficient to control other factors not explicitly captured in the optimization. It is profitable to observe the effects of optimizing specific turbine or WP variables on others to take advantage of these relationships to cater to more factors not captured in the optimization problem but correlated with those captured.

Accurate prediction of turbine wake behavior is critical to power loss attenuation and overall improvement in plant efficiency [1]. Several experimental, numerical [2], and analytical studies [1], [3], [4] have provided insight into turbine wake modeling and effects, with both experimental and numerical models offering high-fidelity solutions compared to analytical methods. On the other hand, the need for simplicity, speed, and reduced computational costs have tilted the preference to static and semi-static models in wake prediction and control studies, while according to [5], CFD-based analytical models well suited for model parameter(s) tuning and control validation purposes. These models have been applied both in simulation studies and

The associate editor coordinating the review of this manuscript and approving it for publication was Ahmed A. Zaki Diab.

for wind plant deployment to optimise the WP performance through layout optimisation, WP power optimisation, as well as fatigue load reduction. Most of these studies focus only on power optimisation, with very few incorporating fatigue load considerations, but only one study with additional extreme load considerations, as seen in [6]. According to [6], cumulative turbine thrusts is the main driver of extreme loads, and a direct relationship exists between a turbine's thrust and its thrust coefficient. A previous study by [7] on WP optimisation of turbines' axial induction factors (α) for annual energy production (AEP) maximisation shows that power maximisation increases turbines' thrust coefficient (C_T) and turbine-level turbulence intensities (TIs). They also demonstrated that increased turbines' C_T values could result from increasing turbine-to-turbine distances. Given the direct relationship between turbine thrust coefficient, thrust, and extreme loads, it could be beneficial to control extreme loads by simply controlling individual turbines' CT values.

The main contribution of this study is to constrain turbine CT values while maximizing WP AEP, and simultaneously investigate the effects of this constraint on AEP, and on turbines' TI levels.

II. RELATED WORKS

A quasi-steady WP flow model presented in [8] shows that both the blade and the tower bending moments can be estimated based on a turbine's C_T value and depend on it. Moreover, the cummulative thrusts on turbines' according to the study in [6] are the principal driver of extreme loads on these turbines. Exceeding the manufacturer's design C_T specification for each freestream inflow, U_∞ could result in more energy being harvested from the wind, as demonstrated in [7]. However, the implications of this would be overexertion due to excessive thrusts, and a possible transfer of mechanical loads into the electrical system.

A centralized WP control using the modified version of the flow re-direction and induction in steady-state (FLORIS) model is presented in [9]. Turbine yaw angles were optimised for all wind speeds in each wind direction, with an already optimised turbine layout as a starting-point. AEP gains of 3.8% and 5.9% are recorded compared to the layout-only optimisation and the base case (original layout, no optimisation), respectively. However, the Gaussian wake model employed in this study does not capture the possible loading effects that could arise through overexertion or increased turbine-level TIs within the WP. A counterpart study [10] uses the same wake model and WP data to achieve a recognizable AEP increase. However, it acknowledges and recognises the possibility of increased loading due to intentional turbine yaw offset through obtained results.

In [11] WP layout is optimised considering the effect of atmospheric stability. Results demonstrate that atmospheric conditions critically influence WP layout optimisation. Given the utilised wind turbine hub height $z_0 = 60m$ and rotor diameter $D = 40m$ for the ideal case and $z_0 = 70m$ and $D = 80m$ for the real WP case, this consideration is necessary, as the turbine rotor which will be at approximately $((D/2) + z_0)$ meters (i.e 80 m and 110 m, respectively) can be considered to be within and very close to the atmospheric boundary layer, assuming an adiabatic temperature profile. Hence, the wind speed profile at such heights is expected to align with the logarithmic fit [12]. The authors fail however, to consider and incorporate load reduction into their study, considering that the vertical mixing between air moving horizontally at different layers within this region can increase turbulence and turbine loads.

A comparative analysis of several previous studies to improve grid-based WPs is seen in [13]. To normalize all turbine heights employed in these studies, the authors assume a flat topography and apply the wind profile power law while applying a unified turbine hub height of 60m. A significant drawback from the compared works is that a constant C_T value of 0.88 was maintained for all turbines. The comparative analysis however, resolves this drawback by applying rotor wind speed-specific C_T values, $C_T(\bar{U})$ for analysis and optimisation of the different layouts. With this upgrade, a significant improvement in WP efficiency was obtained for all layouts analysed. The results showed that the gains offered by constant T-2-T distances in specific directions were lost. Moreover, turbine loads were not considered in this work.

A comprehensive study on the ability of different implementations of the GA algorithm to jointly improve WP power and reduce cost of energy (COE) is given in [14]. Authors introduce a ''bi-criteria identification and relocation (BCIR) mechanism'' into the conventional GA to relocate least efficient turbines and worst blocking turbines while finding the best layout of turbines in a WP. Although results show significant improvement in WP power, COE and WP efficiency, the wake model incorporated even though a 2-D Gaussian wake model, does not possess wake skew properties. The study also does not consider possible extreme loading effects which could arise due to power increments irrespective of the U_∞ values studied, as observed in [7].

A field experiment is embarked upon in [15] using the analytical model in [3] which predicts turbine power production based on turbine yaw angle offsets and the atmospheric conditions around the turbines. Obtained results show power increments of between 47% and 7% depending on the freestream, U_∞ - with higher U_∞ values (7 - 8 m/s) yielding a lower power increment while lower U_∞ values (5 - 6 m/s) yield higher power increments. In their model, no consideration was given to possible loads on yawing turbines. Moreover, the model does not capture the inherent wake skew observed in [16] and [17]. An upgraded version of the model in [3], proposed in [18] and which is further capable of predicting TI-levels at turbines is applied in a counterpart study in [19] aimed at optimising turbine yaw offset angles to improve WP power and reduce turbine loads. The study falls short by not accounting for the inherent skew in a rotating turbine' wake. It utilizes a constant ambient TI

for load predictions, which is not characteristic of a typical WP reality.

The model employed by [20] does incorporate TI estimations and control in optimizing WP energy. Their study combines axial induction control with wake steering control methodologies. However, it applies a very simplified wake combination method for multiple wakes - opting to consider only the highest velocity deficit turbine as the total deficit on a downstream turbine, irrespective of the number of turbines upstream. Moreover, the study applies a wake deflection model that has a rectangular instead of Gaussian wake profile, offering it a low fidelity compared to recently developed models in [1], [3], and [4] who also apply more advanced wake combination methods as studied in [18] and [21].

Considering findings in the literature, this study employs an actual turbine with real-site wind data to maximise the AEP of a WP, while constraining the C_T values of individual turbines to within manufacturer specifications. The thrust exerted by these turbines directly depends on these C_T values. Therefore, maintaining a value for each turbine that is within manufacturer specification for the wind speed experienced by the turbine will enhance the healthy operation of that turbine and the longevity of the WP operation. A high-fidelity 2-D Gaussian wake model with yaw and skew capabilities was used to model the wake interactions in the WP. This model is coupled with an augmented version of the simplified implementation of Frandsen's TI model [22] studied in [23], to also account for and observe TI variations due to C_T-contrained AEP maximisation.

III. WIND PLANT MODELLING AND WAKE ANALYSIS

A. WIND PLANT AND TURBINE MODEL

Given a fixed WP site, turbines are deployed in a hexagonal lattice as depicted in Fig. 1. To observe parameter variations concerning the increase in deployment distance, two scenarios with minimum turbine to turbine (T-2-T) distances $5D$ and $6D$, respectively, are studied. The selected layout has the potential to enable T-2-T distances that are as large as the conventional $7D$ deployment distances in some directions while also enabling tighter T-2-T distances in other directions. This allows the gains of sparse deployments such as reduced wake deficits to be enjoyed, while exploiting the increased turbine density enhanced by tightly spaced deployments. To reduce the computational cost, the hypothetical multi-directional WP studied is split into 12 bins and Table 1 further clarifies other employed WP parameters. 5D hexagonal turbine deployment for bins 0, 1, and 3 are given in Figs. 17 to 19, respectively, of appendix B section.

Assumption 1: The pair (U_∞, θ^W) is constant across the WP length (and in any direction considered), with variations in θ^W having a frequency of hourly intervals.

For all analysis, the variable-wind, variable-pitch, 3-bladed Gamesa-g128-5.0MW turbine publicly available at en.wind-turbine-models.com [24], with given data: Rated power $(P_r) = 5.0$ MW, Cut-in wind speed $(U_{in}) = 3$ m/s, Rated wind speed $(U_r) = 14.5$ m/s, Cut-out wind speed $(U_{out}) = 27$ m/s, Rotor diameter $(D) = 128$ m, Hub height $(z_0) = 140$ m, is used.

TABLE 1. Wind plant parameters.

Parameter	Meaning	Value	Unit
$\mathcal{A}$	Farm Area	4655 x 2880	m^2
T-2-T spacings	Minimum spacings between turbines	5, 6	D
$\mathcal{N}$	Total number of turbines	$6D = 32$ $5D = 45$	
bins	Wind directions $\pm 15°$	12 (0 - 11)	°

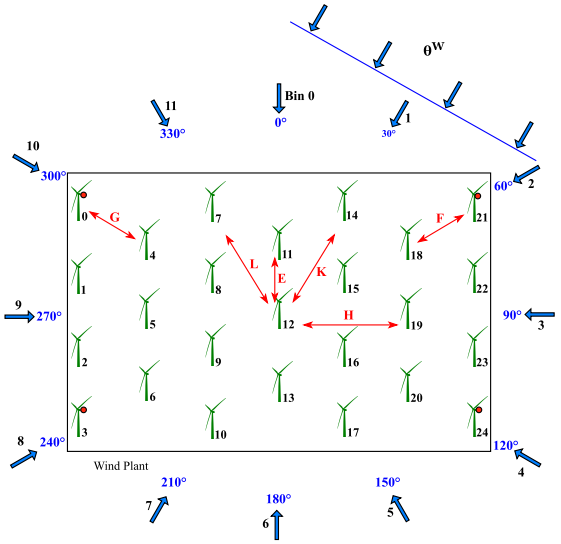

FIGURE 1. Wind plant layout showing turbines in a hexagonal lattice.

B. WAKE MODEL

Given the need to advance real-time solutions, this study employs the continuous and differentiable analytical wake model proposed in [4] which has a Gaussian shape in axial and radial directions, to model the single and multiple wake scenarios. Consider a row of turbines $i, j, \ldots, n$ at locations $l_i = (x_i, y_i)$, $l_j = (x_j, y_j), \ldots, l_n = (x_n, y_n)$ where n is the furthest downstream turbine and i the furthest upstream turbine facing an arbitrary wind direction θ^W and experiencing the freestream wind speed U_∞. According to the authors, the distance between i and j can be expressed using two parameters; the axial T-2-T distance $d_{j,i}$, and the radial T-2-T distance $r_{j,i}$, respectively, of j relative to i, as shown in Figs. 2 and 3. Hence, $d_{j,i}$ can be computed as thus:

$$d_{j,i} = ||l_j - l_i||_2 \cos(|\theta_{j,i} - \theta^W|) \tag{1}$$

where $||l_j - l_i||_2 = ((x_j - x_i)^2 + (y_j - y_i)^2)^{1/2}$ is the the euclidean norm and $\theta_{ji} = \tan^{-1}((x_j - x_i)/(y_j - y_i))$ is the angle between turbines i and j.

The effective radial T-2-T distance $r_{j,i}$ is then expressed in [17] as a sum of all the radial components as given:

$$r_{j,i} = r^l_{j,i} + r^r_{j,i} + r^\phi_{j,i} sign(\theta_{j,i} - \theta^W), \tag{2}$$

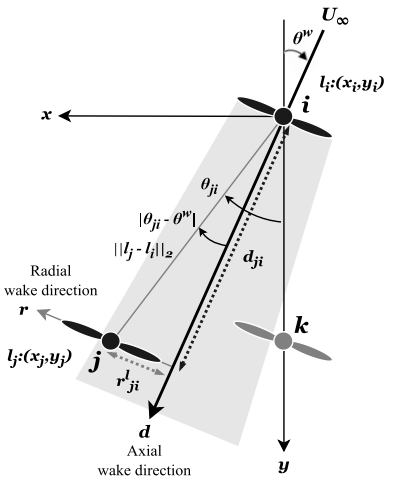

FIGURE 2. Axial T-2-T distance $d_{j,i}$, and $r^l_{j,i}$ [16].

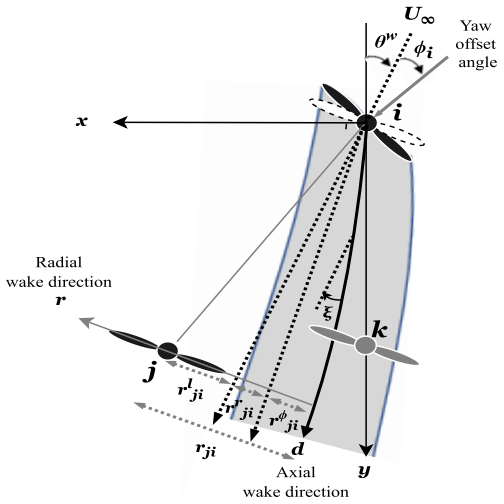

FIGURE 3. Radial T-2-T distance $r_{j,i}$ [4].

where $r^l_{j,i}$ (the location-induced radial T-2-T distance) is defined mathematically as:

$$r^l_{j,i} = ||l_j - l_i||_2 \sin(|\theta_{j,i} - \theta^W|), \tag{3}$$

It is observed in [16] and [17] that the wake formation behind a rotating turbine is marginally skewed even without yaw. This intrinsic skew causes an additional radial T-2-T distance known as the blade rotation-induced T-2-T distance, $r^r_{j,i}$:

$$r^r_{j,i} = \psi d_{j,i} = \psi ||l_j - l_i||_2 \cos(|\theta_{j,i} - \theta^W|), \tag{4}$$

where ψ is the slope of the skewed wake axis. It has been well-established via experimental studies [25] and CFD simulations [2], [26] that offsetting the yaw angle of a turbine can initially redirect the wake away from the path of the freestream inflow, deflecting it in the direction opposite to the yaw rotation [26]. Yawing deflects the wake, causing the wake axis to be skewed from the normal (*w.r.t* the zero-yaw rotor position) by an angle $\xi(d)$. Hence, [17] defines this skew angle at a downstream distance d, $\xi(d)$, in relation to the yaw offset ϕ, the axial induction α of the upstream turbine, and its thrust coefficient C_T in zero-yaw conditions as:

$$\xi(d) \approx \frac{\cos^2(\phi_i)\sin(\phi_i)\frac{C_T(\alpha_i,\phi_i)}{2}}{(1+\frac{2\tau d}{D})^2}, \tag{5}$$

where the numerator represents the initial skew angle of the wake axis just behind the rotor (*i.e.*, $d = 0$ and the wake width $\approx D$), τ is the model parameter that controls the wake deflection's sensitivity to yawing. The yaw-induced radial T-2-T distance $r^\phi_{j,i}$ is then expressed by [17] in (6). Fig. 3 encompasses all components of the radial T-2-T distance.

$$r^\phi_{j,i} = \int_0^{d_{j,i}} \tan(\xi(d))\, dx \quad . \tag{6}$$

Using local polar coordinates (r', θ'), [4] expresses the deficit at any point on the rotor surface of a downstream turbine as:

$$U_{def_{j,i}}(d_{j,i}, r, \alpha_i, \phi_i) = 2\alpha \left(\frac{R}{R+kd}\right)^2 \exp\left(-\left(\frac{r}{R+kd}\right)^2\right), \tag{7}$$

where R is the rotor radius, k is the wake expansion rate, r is expressed as $\sqrt{(r_{j,i} - r'\cos\theta')^2 + (r'\sin\theta')^2}$ and d as $d_{j,i}$. Then, at a downstream location (d, r), the wind speed at any point (r', θ') on a downstream rotor surface is given as:

$$m_1 = \begin{cases} (1 - U_{def_{j,i}}(d_{j,i}, r, \alpha_i, \phi_i))U_\infty, & \text{if } d_{j,i} \geq 0 \\ U_\infty, & otherwise. \end{cases} \tag{8}$$

where $m_1 = U_{j,i}(r', \theta', \alpha_i, \phi_i; U_\infty, \theta^W)$. The averaged wind speed on the entire rotor surface is given as:

$$\bar{U}_{j,i}(\alpha_i, \phi_i; U_\infty, \theta^W) = \frac{1}{\pi R^2} \int_{\theta'=0}^{\theta'=2\pi} \int_{r'=0}^{r'=R} m_1 r'\, dr' d\theta', \tag{9}$$

The generalized power of a controlled turbine j due to i, is then defined based on [27] as:

$$m_2 = \begin{cases} 0, & \text{if } U_\infty < U_{in} \\ \frac{1}{2}\rho A \bar{U}^3_{j,i}(\alpha_i, \phi_i; U_\infty, \theta^W) C_P(\alpha_j), & \\ \quad \text{if } U_{in} \leq U_\infty < U_{out} & \\ 0, & \text{if } U_{out} \leq U_\infty, \end{cases} \tag{10}$$

where $m_2 = P_{j,i}(\alpha_i, \alpha_j; U_\infty, \theta^W)$, and C_P the power factor.

For simplicity all turbine yaw angles, ϕ, are preset to 0°, $\forall i \in \mathcal{N}$, to maintain focus on constraining turbine C_T values and observing the resultant effects on AEP and TI levels. Due to concurrent wakes from multiple turbines, the aggregated deficit on a downstream turbine j is generalized as:

$$\bar{U}_{def_j}(\boldsymbol{\alpha}; \theta^W) = \sqrt{\sum_{i=1}^{\mathcal{I}} (\bar{U}_{def_{j,i}}(\alpha_i; \theta^W))^2} \tag{11}$$

where $\mathcal{T}$ is the total number of turbines in the upstream of j, $\boldsymbol{\alpha}$ is the axial induction factor vector of all upstream turbines' axial induction factors (i.e, $\boldsymbol{\alpha} = (\alpha_1, \ldots, \alpha_{\mathcal{T}})$)

Finally, given a wind condition (U_∞, θ^W), the averaged wind speed at a downstream rotor can be computed as:

$$\bar{U}_j(\boldsymbol{\alpha}; U_\infty, \theta^W) = (1 - \bar{U}_{def_j}(\boldsymbol{\alpha}; \theta^W))U_\infty, \tag{12}$$

and the power of any downstream turbine, j, can be expressed as a function of the control actions α of all upstream turbines i ahead of j in the direction considered:

$$P_j(\boldsymbol{\alpha}; U_\infty, \theta^W) = \frac{1}{2}\rho A \bar{U}_j^3(\boldsymbol{\alpha}_{-j}; U_\infty, \theta^W)C_p(\alpha_j) \quad . \tag{13}$$

The WP power $P_{\mathcal{N}}$ is then computed as a sum of the power generation from all $\mathcal{N}$ turbines in the WP as:

$$P_{\mathcal{N}} = \sum_{j=1}^{\mathcal{N}} P_j(\boldsymbol{\alpha}; U_\infty, \theta^W) \quad . \tag{14}$$

C. TURBULENCE INTENSITY MODEL

According to the IEC standard 61400-1 edition 3 [28] which drafts the minimum requirements for fixed offshore wind turbines, the effective TI at any location (d, r) within a site can be estimated from the 90^{th} percentile value of turbulence in the wind, measured at every 10-minute interval for a considered wind direction θ^W (with a typical sampling frequency of 1-2 seconds). Based on this 90th percentile value of turbulence also known as the representative standard deviation (σ_{repr}), and the freestream inflow, U_∞, Frandsen [22] develops equations for computing TI for both the representative (σ_{repr}) and mean values (σ_{mean}) of the distribution. An in-depth study and explanation of these equations can be seen in [23]. The authors in [7] due to the minimum T-2-T distance considered in their study ($5D$) made augmentations to the expression for computing σ_{mean} in Frandsen's "wake turbulence" (WT) model (15), by replacing U_∞ with U_j to reflect local conditions within the WP as given in (16). It is pertinent to point out that the T-2-T distance studied in [7] meets the requirement by Frandsen to apply the WT model - a model which assumes no ambient wind farm turbulence regardless of a turbine's position in the WP due to the T-2-T distance.

$$\sigma_{\infty,wake} = \sqrt{\frac{{U_\infty}^2}{\left(1.5 + 0.8\left(\frac{d_{norm}}{\sqrt{C_T}}\right)\right)^2} + \sigma^2_{mean,\infty}}, \tag{15}$$

where $\sigma^2_{mean,\infty}$ is the mean of the 10-min standard deviation values squared, and d_{norm} (defined mathematically as $d_{j,i}/D$) is the normalized axial T-2-T distance between i and j.

$$\sigma_{j,wake} = \sqrt{\frac{\bar{U}_j^2}{\left(1.5 + 0.8\left(\frac{d_{norm}}{\sqrt{C_T}}\right)\right)^2} + \sigma^2_{mean,\infty}}, \tag{16}$$

Furthermore, Frandsen's equation for border turbines (turbines that experience the freestream inflow due to their positions) as given in (17) makes no provision for turbine parameter variation in the case of optimisation purposes.

$$\sigma_{mean,\infty} = \langle \sigma_\infty \rangle, \tag{17}$$

Consequently, [7] opts to apply Frandsen's inner turbine equations for border turbines as given in (15). The parameter d_{norm} is then computed as $1000D/D$ for border turbines, to reflect a hypothetical upstream turbine assumed to be very far away from the considered turbine (denoting an almost non-existent upstream turbine). This decision which has been well-explained and validated in [7], produced comparable σ and, consequently, TI results. Hence, for all TI analysis in this study, the augmented equations for border and inner turbines - (15) and (16), respectively, as proposed in [7] are employed, and focus is laid on mean TI, not representative TI. Mean TIs at turbines can then be computed as:

$$TI = \frac{\sigma(\theta, U_\infty)}{U_\infty}, \tag{18}$$

where $\sigma(\theta, U_\infty) \equiv \sigma_{\infty,wake} \equiv \sigma_{j,wake}$.

IV. OPTIMIZATION PROBLEM FORMULATION

This section presents a coordinated control of a WP for AEP maximisation and confinement of turbine thrust coefficient within manufacturer specified optimal levels. The mean wind speeds available at each downstream turbine's ($j's$) rotor depends on the axial induction α of all the turbine's $i's$ in its upstream. This resulting mean wind speed $\bar{U}_j$ then determines the thrust coefficient of j and the corresponding thrust force that it exerts on the inflow. Given that each mean wind speed has a corresponding optimal C_T value for the optimal output power at that wind speed to be realised, it is paramount to ensure that while optimizing the α all turbines to maximise AEP, the optimiser be constrained to randomly select α values for each turbine that is not above the corresponding α value of the U available at each turbine - which ultimately depends on the α values of all its upstream turbines.

Consider that wind is blowing uniformly into a bounded hypothetical multi-directional wind plant (WP) from each direction per instance, as shown in Fig. 1, and can vary both in speed and direction albeit slowly. Let $\mathcal{N}$ be a set of all turbines in the wind plant, $\mathcal{B}$ a set of all wind directions/bins, $\mathcal{U}$ a set of operating wind speeds for all wind turbines, and $\mathcal{T}$ is a set of turbines upstream of each turbine - this set being direction-dependent.

The AEP is computed as the weighted sum of the total WP power for each wind bin, P_b, across all operating wind speeds, $\mathcal{U}$, for all turbines, $\mathcal{N}$. The weighting is provided by the frequency of occurrence of each bin, f_b, multiplied by the number of hours in the year, N_h.

$$AEP = N_h \sum_{b=1}^{\mathcal{B}} \sum_{u=1}^{\mathcal{U}} \sum_{j=1}^{\mathcal{N}} P_{b,u,j} * f_b \tag{19}$$

The optimisation problem can be formulated as thus:

$$\begin{aligned} \max_{(U_{b,u,j}, P_{b,u,j})} \quad & AEP \\ \text{s.t.} \quad & \bar{U}_j \leq U_\infty \\ & C_{Tj} \leq C_T{}^{\bar{U}_j}. \end{aligned} \tag{20}$$

Given the choice to set $\phi = 0°$ $\forall i \in \mathcal{N}$, $P_{b,u,j}$ is expressed in its closed form as:

$$P_{b,u,j}(\boldsymbol{\alpha}; U_\infty) = \frac{1}{2}\rho A \bar{U}^3_{b,u,j}(\boldsymbol{\alpha_{b,u,-j}}; U_\infty) C_p(\alpha_{b,u,j}). \tag{21}$$

Constraint 1 in (20) ensures that the mean wind speed available at each turbine's rotor, $\bar{U}_j$, after wake contributions from upstream turbines, does not exceed the freestream wind inflow into the WP, U_∞. Additionally, constraint 2 in (20) restricts the thrust coefficient of each turbine, C_{Tj}, from exceeding the thrust coefficient synonymous with the mean wind speed at the turbine's rotor, $C_T{}^{\bar{U}_j}$. The thrust coefficient and power coefficient curves indicate the baseline operating limit of a turbine within the cut-out wind speed, taking into consideration its mechanical and electrical system. Hence, constraints 2 ensures that the turbine remains within such operational bounds, to prevent overexertion of the turbine mechanical systems, which could lead to increased loading.

V. NUMERICAL RESULTS

The wake (13) and TI (18) models are employed for both the *Base* and optimised cases (*PSO* and *GA*), to compute turbine power and TI levels at turbines. The *Base* case represents the non-optimised case with greedy extraction. The optimised case however, considers downstream turbines, allowing turbines' α values to be adjusted to enhance an improved collective WP power. Variable optimisation is achieved using PSO and GA with the following parameters: PSO $-$ $\{c1 = 1.8, c2 = 1.5, wMax = 0.9, wMin = 0.2\}$; GA $-$ $\{pc = 1, gamma = 0.1, mu = 0.01, sigma = 0.1$, Selection $= Random\}$, $pop\_size = 20$, $MaxIter = 500$. System model development is implemented on version 3.9 of the python programming environment. For optimisation, the PSO model is developed by [29], and the GA algorithm can be seen in [30]. These meta-heuristic algorithms have been applied extensively with success in the field to yield improvements both in regular and irregular layouts as attested to by the review in [31].

Table 2 is based on Figure 1, and shows the studied scenarios and the resulting T-2-T distances in other directions. Performance comparisons are made between the base-case (*Base*), the unconstrained optimised cases using PSO and GA (*PSO*, *GA*), and the constrained optimised cases (*PSO_CT*, *GA_CT*), for each scenario, and for mean inflow wind speeds from U_{in} up to U_r and are shown in Table 2.

A. POWER ANALYSIS

Figs. 4 and 5 show the total WP power based on bins and U_∞ values. The plots demonstrate that thrust coefficient constraints inhibit overall WP power generation.

TABLE 2. Studied T-2-T separation distances in rotor diameters.

Minimum T-2-T Distance (D)	$E = F = G$	$H = K = L$
5	5	≈ 8.66
6	6	≈ 10.4

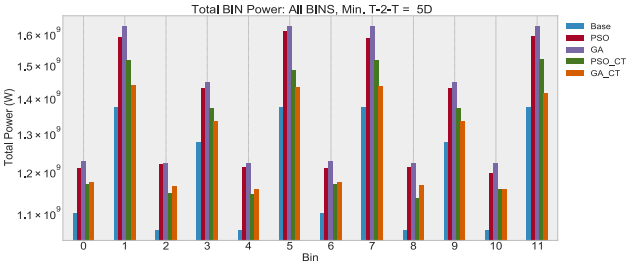

FIGURE 4. Total bin powers for a 5*D* minimum T-2-T distance.

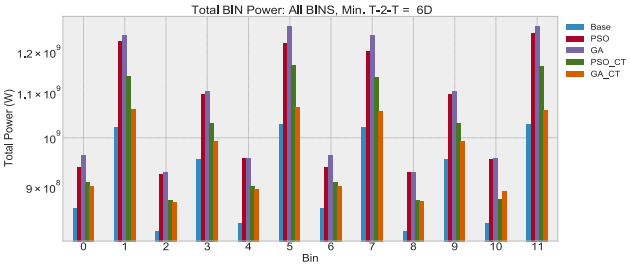

FIGURE 5. Total bin powers for a 6*D* minimum T-2-T distance.

They also demonstrate that odd-numbered bins - which have sparse T-2-T separation, yield a more considerable total WP power. A disparity between odd-numbered bins is observed, where bins 3 and 9 have a lower total WP power than to 1, 5, 7, and 11. Referencing Figs. 18 and 19 in the Appendix B section, this disparity can be attributed to the "shallow array" property exhibited by bins 1, 5, 7, and 11 where turbine columns comprise a maximum of four turbines. Whereas, turbine columns in bins 3 and 9 comprise up to five turbines, causing more significant cumulative wind speed deficit for far downstream turbines and a more considerable reduction in turbine-generated power. Consequently, this translates to a reduced total WP power generation. Furthermore, compared to bins 3 and 9 which have nine (9) turbine columns, bins 1, 5, 7, and 11 have seventeen (17) turbine columns, resulting in 17 border turbines. Hence, these bins have a more significant number of turbines privy to the freestream wind inflow, which is devoid of any deficit since no turbine is upstream. The implication is more border turbines that contribute more power to the total generated WP power.

B. AEP ANALYSIS

Table 3 presents the AEP from all bins for the 5D scenario, while Table 4 compares the total AEP and percentage increments between the 5*D* and 6*D* scenarios. Irrespective of the total bin powers illustrated in Figs 4 and 5, a high bin power does not automatically translate to a high bin AEP. The AEP is seen to be more dependent on the bin probabilities

TABLE 3. AEP table for 5*D*.

	Base AEP(TWh)	**PSO** AEP(TWh)	**GA** AEP(TWh)	**PSO_CT** AEP(TWh)	**GA_CT** AEP(TWh)
bin 0	90.26	98.98	100.5	95.83	96.11
bin 1	70.80	81.91	83.86	78.11	74.08
bin 2	98.89	113.3	113.7	106.8	108.4
bin 3	108.1	120.9	122.5	116.1	112.9
bin 4	65.08	74.17	74.75	70.08	70.87
bin 5	91.21	106.9	108.0	98.57	95.04
bin 6	92.29	101.2	102.8	98.00	98.28
bin 7	97.86	113.0	115.9	108.0	102.3
bin 8	58.40	66.58	67.09	62.41	64.10
bin 9	84.37	94.42	95.68	90.69	88.16
bin 10	86.53	97.37	99.43	94.13	94.25
bin 11	108.9	126.2	129.1	120.4	112.2
Total AEP ≈	**1053**	**1195**	**1213**	**1139**	**1117**
Increase (%)	0	11.91	13.25	7.59	5.74

TABLE 4. Summary AEP table for all studied scenarios.

	Base AEP(TWh)	**PSO** AEP(TWh)	**GA** AEP(TWh)	**PSO_CT** AEP(TWh)	**GA_CT** AEP(TWh)
Total AEP (5*D*)	**1053**	**1195**	**1213**	**1139**	**1117**
Increase (%)	0	11.91	13.25	7.59	5.74
Total AEP (6*D*)	**802.9**	**924.4**	**938.3**	**872.5**	**841.5**
Increase (%)	0	13.15	14.44	7.98	4.60

as depicted in the windrose (Fig 16 in the Appendix A section). This is why bin 1 (sparsely-spaced with a large total bin power) contributes less to the total AEP, compared to bin 0 (tightly-spaced with a smaller total bin power). Bins 4 and 8, being tightly-spaced and additionally having low bin probabilities contribute least to the total AEP.

C. THRUST COEFFICIENT ANALYSIS

Plots are presented of C_T variations at turbines for all freestream inflow wind speeds U_∞, and for selected bins that are representative of the remaining bins in terms of T-2-T distance.

The freestream inflow U_∞ changes at each instance of time of WP operation, causing corresponding changes in the wake deficits at each turbine from the uppermost row of turbines to the furthest. These wake deficits cause different mean wind speeds $\bar{U}$ at each turbine based on their relative positions, hence different turbine $C_T(\bar{U})$ values (i.e *Control*) for healthy and optimal instantaneous operations. Applying C_T constraints significantly reduces for each U_∞ value, the number of turbines that exceed their control C_T values for healthy operations. The method also reduces the number of U_∞ values with affected turbines (*Optimised* C_T values > *Control* values) as demonstrated in Figs. 6 - 8. About Table 2 and Fig 1 the inter-turbine distance is more prominent for bin 1 (**K**) than it is for bin 0 (**E**) and bin 2 (**F**).

So, comparing corresponding U_∞ value plots across Figs. 6 - 8 that have affected turbines (13 m/s and 14 m/s), it is observed that the number of affected turbines is more significant in bin 1, than in bins 0 and 2. Fig. 9 compares the number of affected turbines at all U_∞ values, across all bins for the 5*D* minimum T-2-T distance, using the GA algorithm to emphasize this observation at each U_∞. Further, the figure shows that at corresponding U_∞ values, the number of affected turbines is greater in the odd-numbered (sparsely-spaced) bins compared to their even-numbered (tightly-spaced) counterparts, for both the unconstrained and constrained cases. These results indicate a positive correlation between sparse deployments and high turbines' C_T values. This correlation could be attributed to the direct proportionality between C_T and d_{norm} (the distance in meters between a considered turbine and its nearest upstream turbine, normalised by the rotor diameter of the upstream turbine) when (15) or (16) is substituted into (18), and C_T made the subject of the formula. So, with other parameters kept constant, increasing d_{norm} will increase the considered turbine's C_T.

A performance comparison between both algorithms is demonstrated in Fig. 10 and the PSO results further validate the trend shown by the GA algorithm.

A closer inspection of Fig. 9, shows that the constraints offer an advantage over the U_∞ range 5 m/s - 12 m/s for both sparsely-spaced and tightly-spaced bins. Below 5 m/s, turbines' *optimised* C_T values are successfully maintained below corresponding *Control* values via optimisation only.

In terms of algorithms, Fig. 10 demonstrates GA's superior performance over PSO in achieving the C_T constraint goal, as it achieves this goal over a wider range of U_∞ values, and with a lower number of defaulting turbines outside such range, for all bins and scenarios. Generally, results indicate a positive correlation between C_T values and minimum T-2-T distances of deployment.

D. TURBULENCE INTENSITY ANALYSIS

The German Institute for Building Techniques (DIBt) recommends that a turbine should have a design lifetime

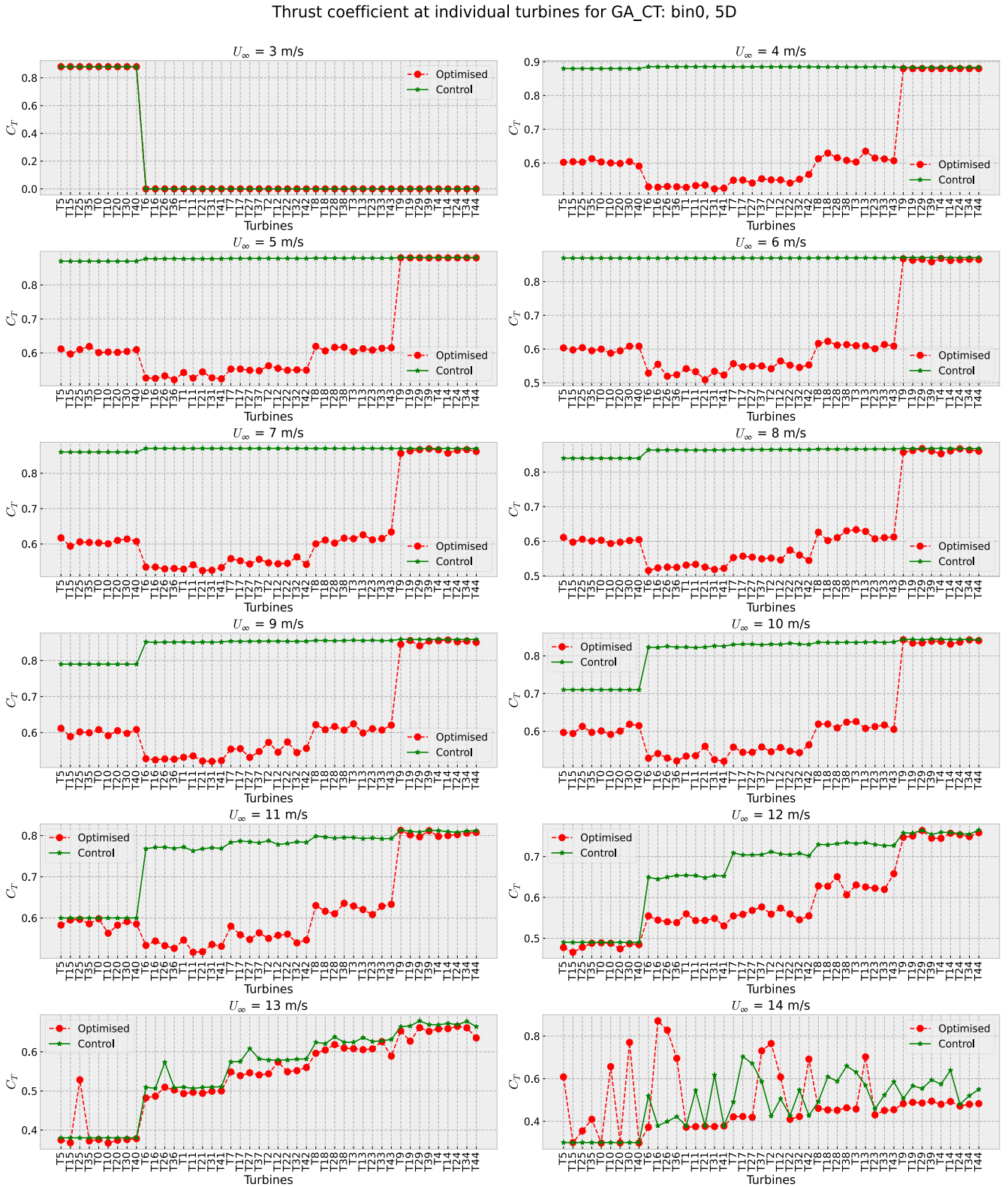

FIGURE 6. **Thrust coefficient at turbines using GA: 5*D*, bin0, U_∞ = 3 - 14 m/s.**

of 20 years in the face of an ambient TI of 20 per cent [32]. Since Frandsen's "wake turbulence" (WT) model albeit slightly augmented, is employed in this study, and this model assumes that the wake-generated turbulence encapsulates all other sources of turbulence because of the T-2-T distances where this model is applicable (<

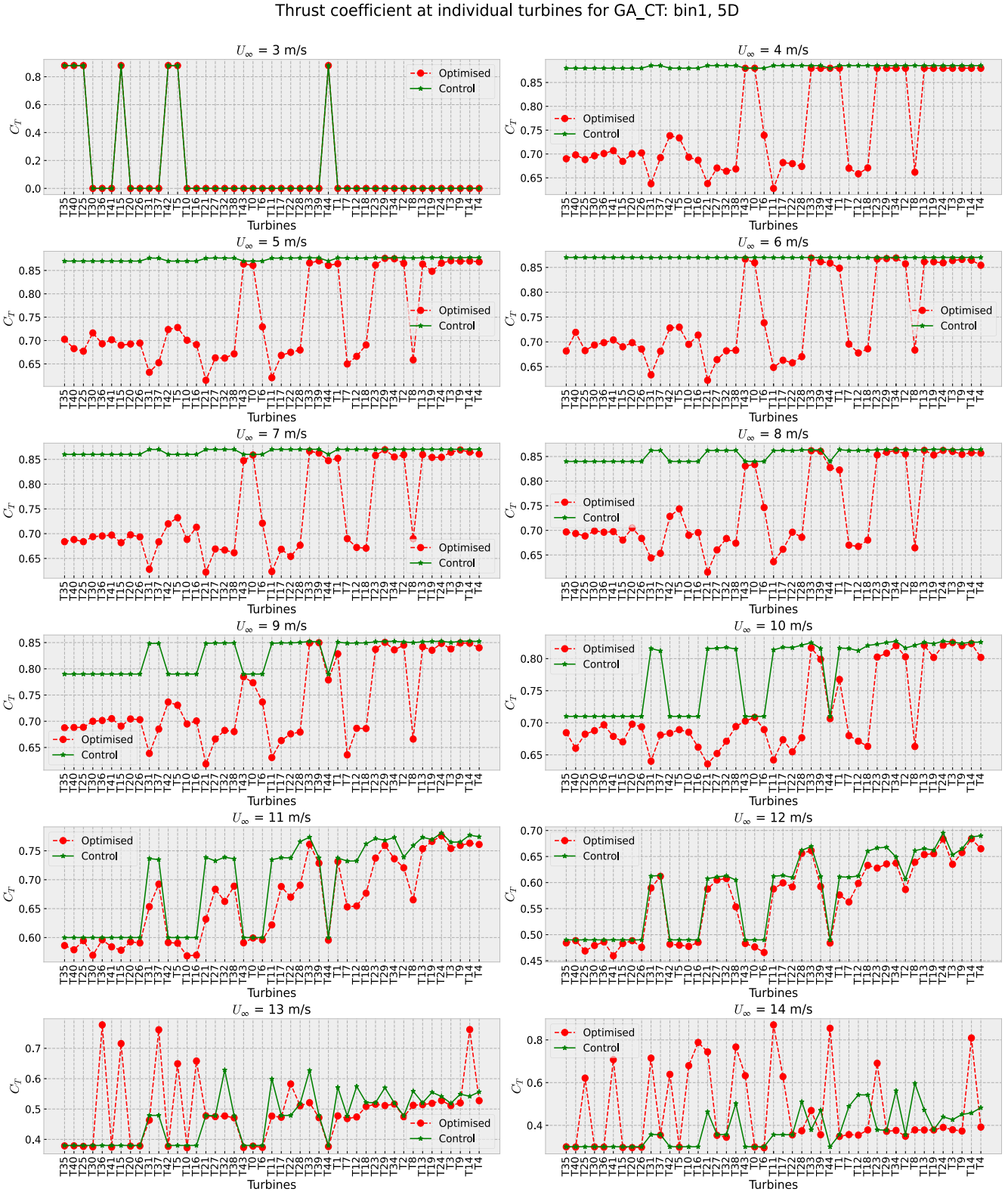

FIGURE 7. Thrust coefficient at turbines using GA: 5*D*, bin1, $U_\infty = 3$ - 14 m/s.

10*D*), this study simply sets the maximum acceptable TI at each turbine (*Threshold*) to 20 per cent. Hence, limiting both border turbines (turbines exposed to the ambient TI) and inner turbines (those exposed to the wake-generated turbulence) to this acceptable TI cap is a reasonable decision.

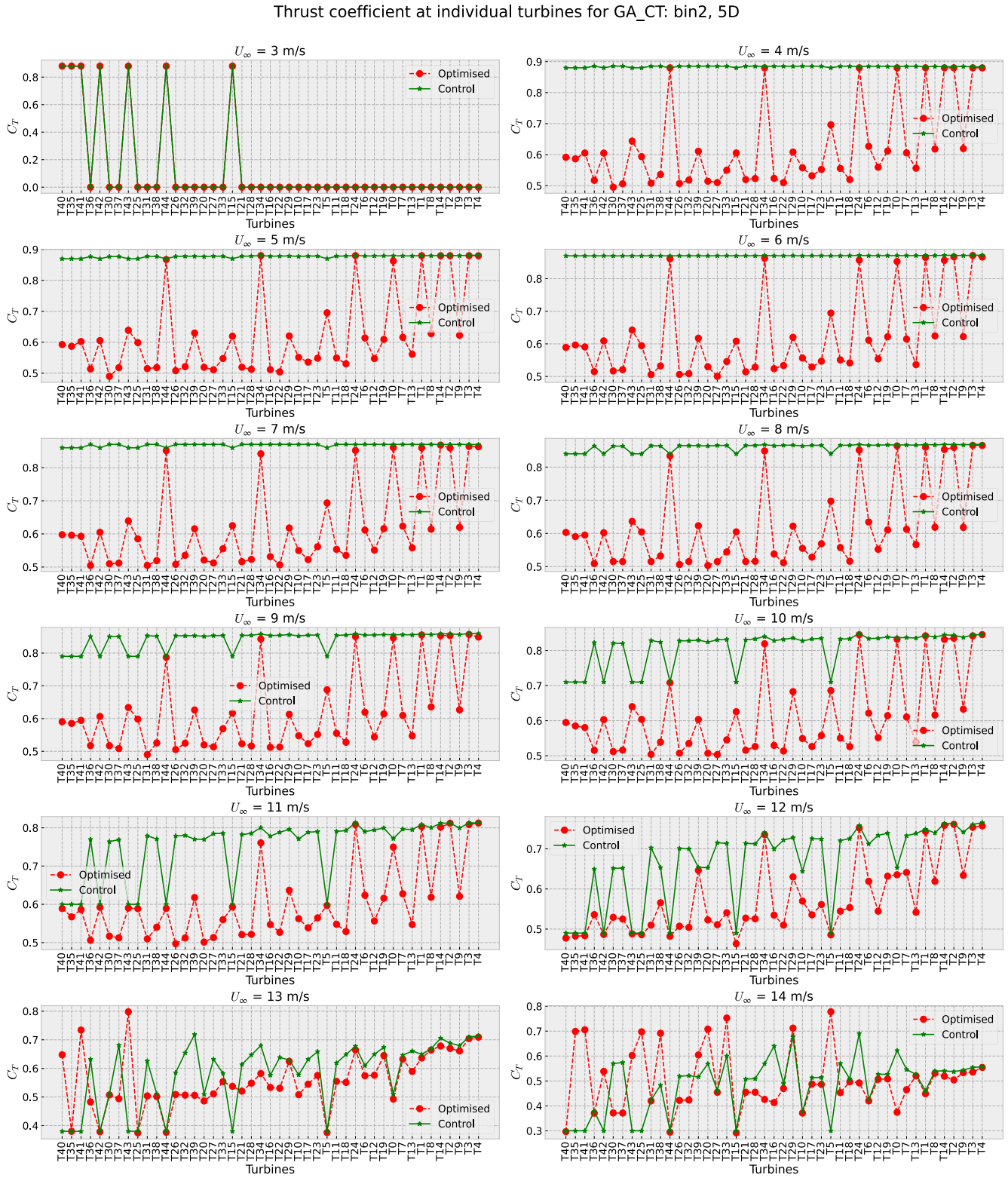

FIGURE 8. **Thrust coefficient at turbines using GA: 5*D*, bin2, $U_\infty = 3$ - 14 m/s.**

To deduce the effects of constraining turbine C_T values on TI levels, the unconstrained (*PSO*, *GA*) and constrained (*PSO_CT*, *GA_CT*) cases are plotted together with the *Base* case and the set threshold TI value. Figs. 11 to 13 show the TI levels by freestream wind speed (U_∞) for all studied cases, for bin 0, 1, and 2.

It is observed that WP power or AEP maximisation with constrained turbine C_T values, pose similar levels of adverse

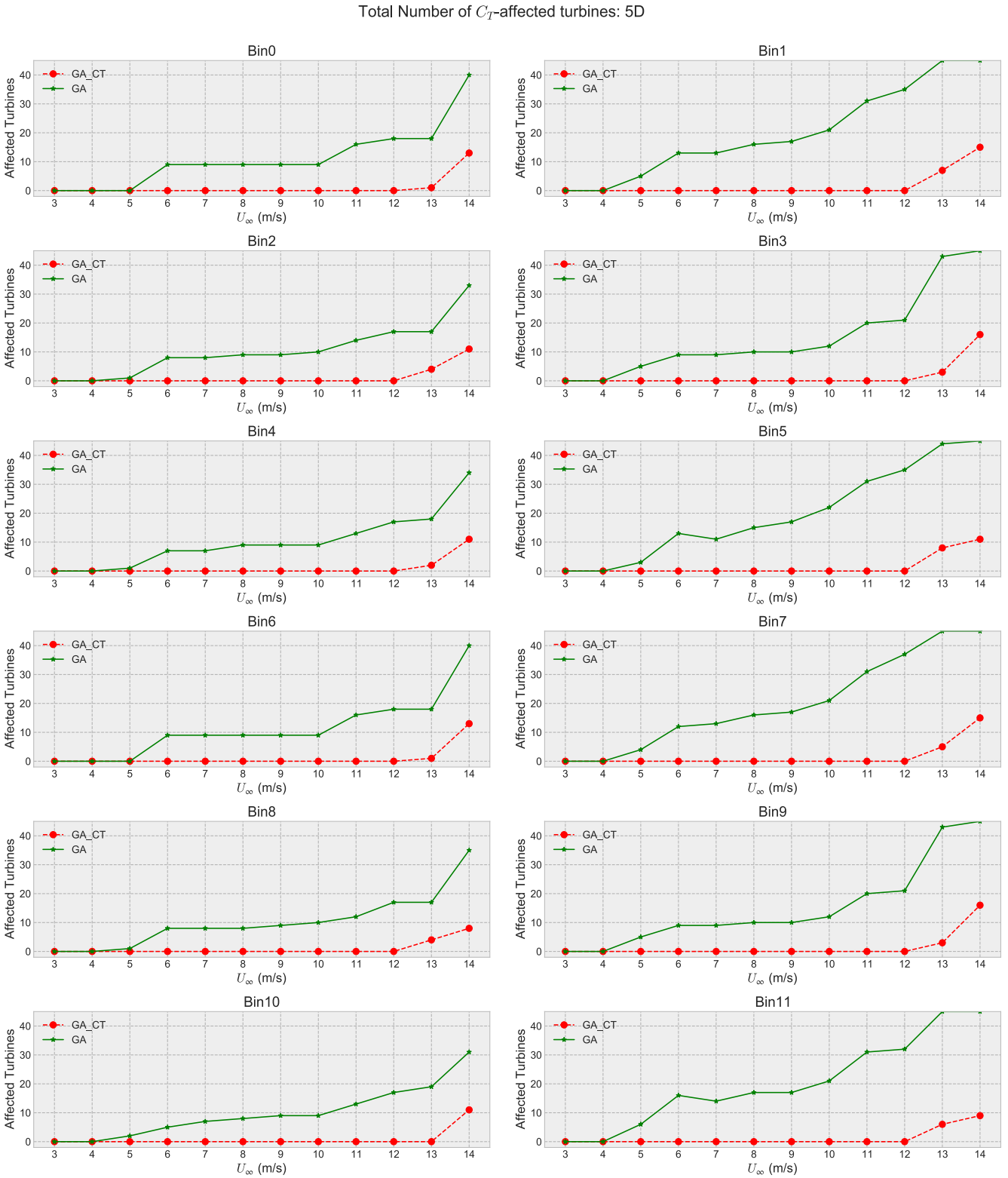

FIGURE 9. Comparison of total affected turbines for constrained and unconstrained cases: GA, 5*D*.

effects on TI levels as without C_T constraints. The box plots for the *Base* case is seen to show a lower range of TI values compared to the optimised cases (constrained and unconstrained).

Figs. 14 and 15 presents box plots of all turbines' TI levels by bin, for 4 m/s and 7 m/s U_∞ values. It is worth pointing out that Bin 0 in Figs. 14 and 15, respectively, is equivalent to TI-levels box plots under 4 m/s and 7 m/s in Fig. 11. For

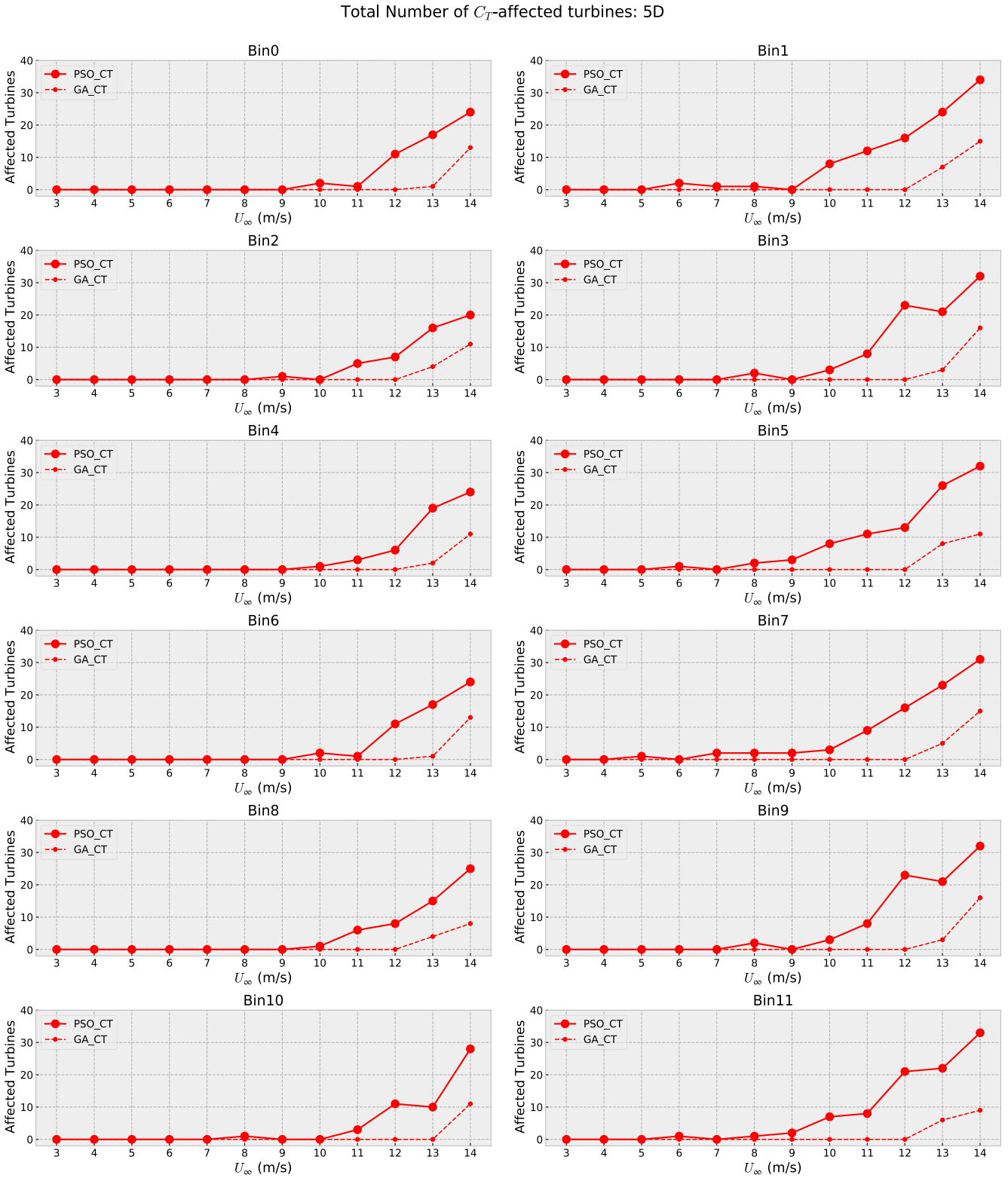

FIGURE 10. **Algorithm comparison for total affected turbines: Constrained cases, *5D*.**

both figures, these increased TI levels are of larger magnitude in tightly-spaced (even-numbered) bins compared to the sparsely-spaced (odd-numbered) bins, inferring and inverse relationship with minimum T-2-T distances of deployment as shown in both 14 and 15. These increased TI levels are shown to decrease with increasing U_∞ values as demonstrated in Figs. 11 to 13. Notwithstanding, TI-levels still exceed the 20% set threshold at U_∞ values up to 7 m/s as seen in Fig. 15.

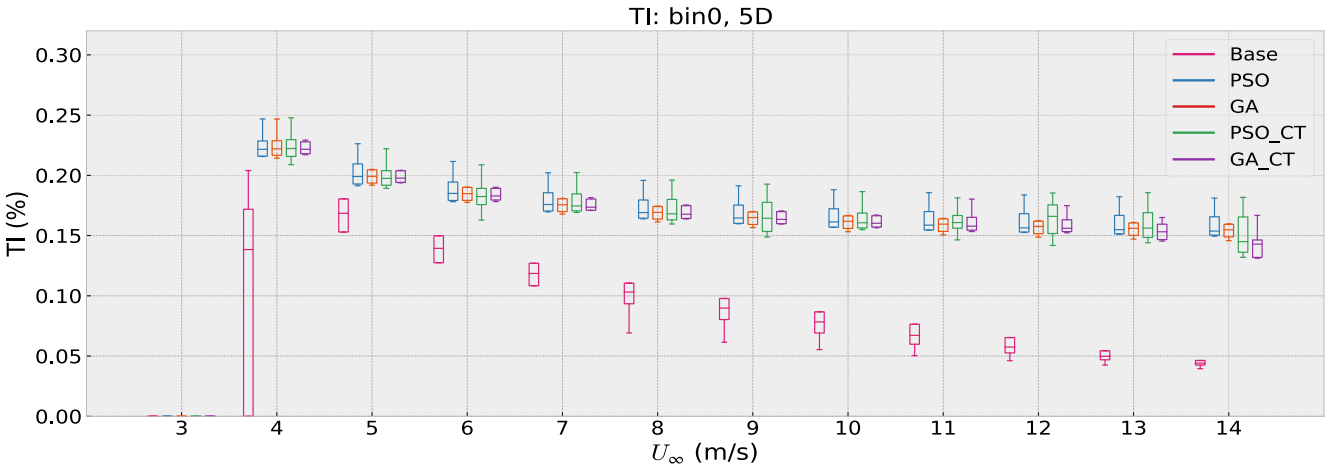

FIGURE 11. Bin 0 at 5*D* minimum T-2-T distance for all U_∞ values.

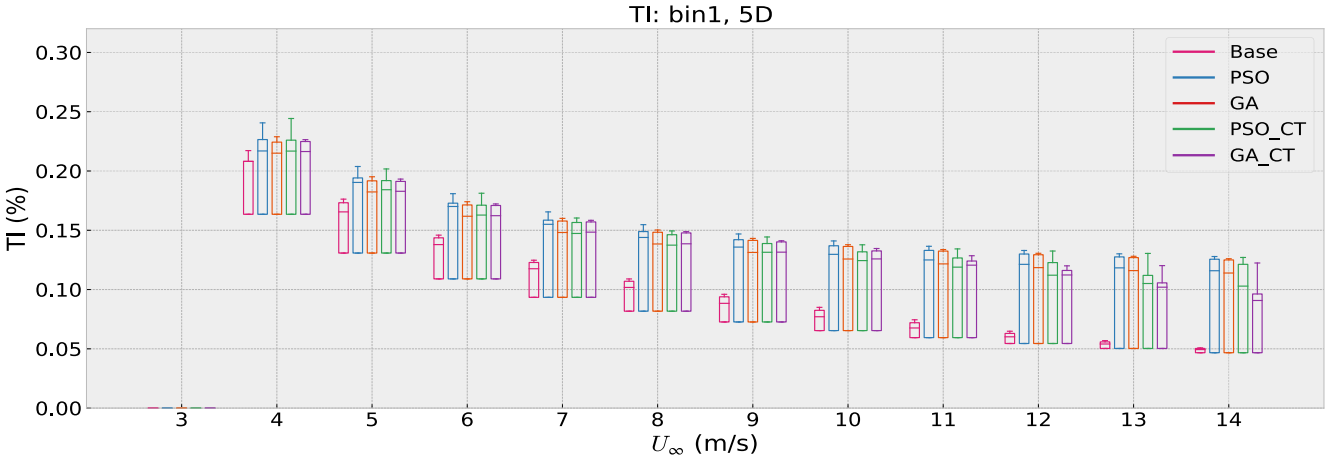

FIGURE 12. Bin 1 at 5*D* minimum T-2-T distance for all U_∞ values .

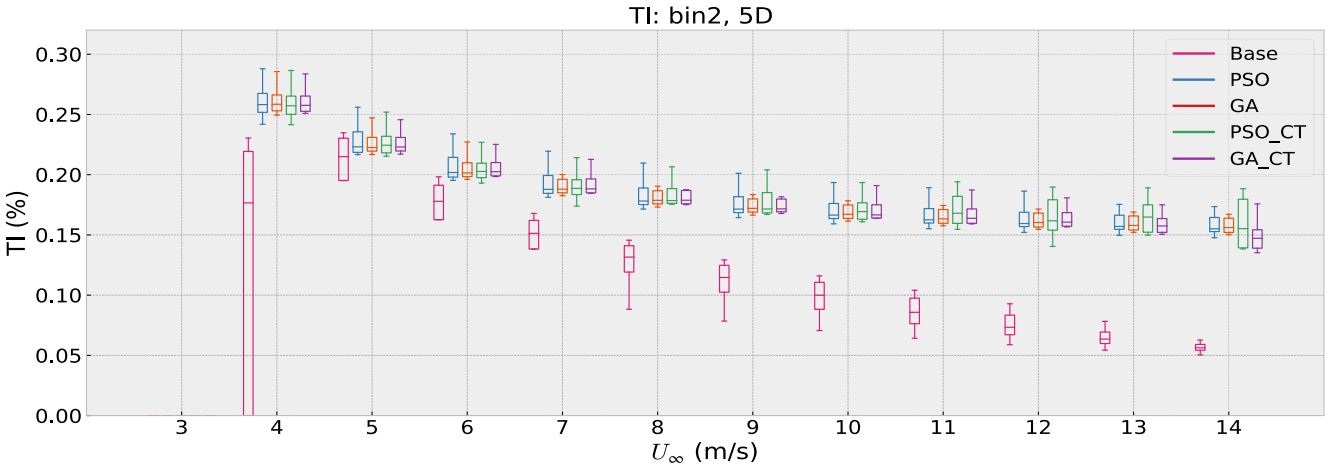

FIGURE 13. Bin 2 at 5*D* minimum T-2-T distance for all U_∞ values .

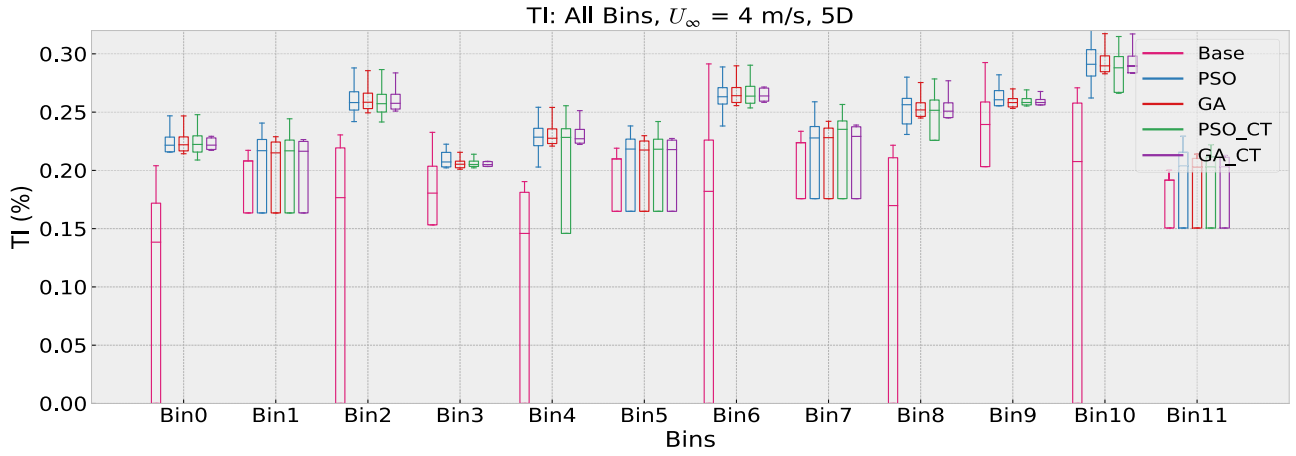

FIGURE 14. Turbulence Intensity for all bins at 4 m/s.

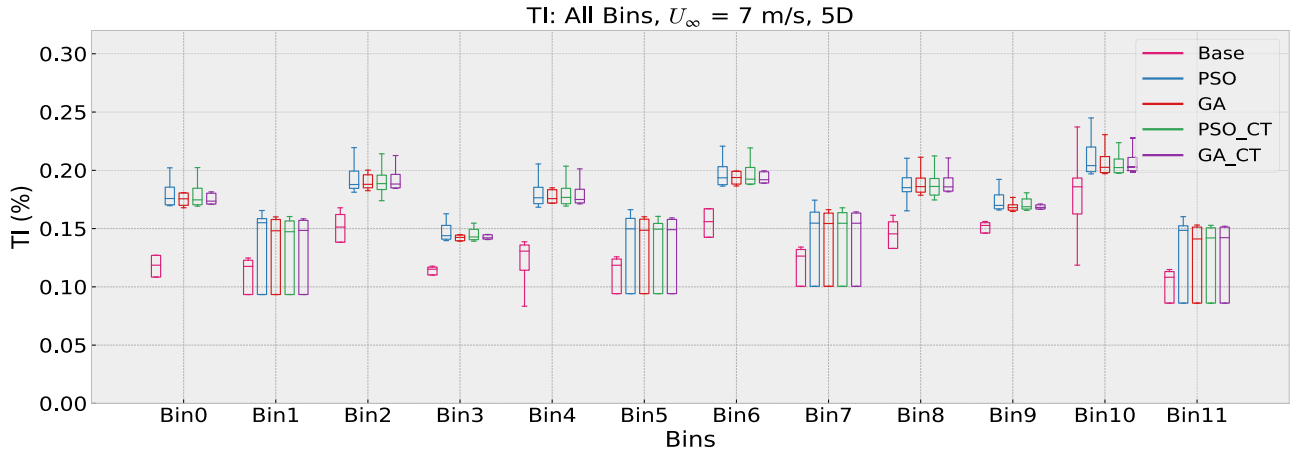

FIGURE 15. Turbulence Intensity for all bins at 7 m/s.

Generally, results indicate a negative correlation between TI levels and minimum T-2-T distances of deployment, but a positive correlation between TI levels and U_∞ values.

VI. CONCLUSION AND RECOMMENDATIONS

A plant-wide thrust coefficient-constrained optimisation of axial induction factors for AEP maximisation was implemented using PSO and GA, and two scenarios (5D and 6D) were compared to observe how a C_T-constrained axial induction optimisation affects the overall AEP and TI-levels within the WP as minimum T-2-T distances is varied.

With C_T values constrained to within manufacturer specifications for each $C_T(\bar{U})$ value, turbines were constrained from overexertion for all values of U_∞ below rated except at 13 m/s and 14 m/s for both sparsely-spaced and tightly-spaced bins. This represents a 66.67% improvement for the GA-applied constrained case when compared to the unconstrained case where turbines' C_T values are observed to be within manufacturer's specification only at $U_\infty = 3$ m/s and 4 m/s, of all twelve U_∞ values studied. This improvement is consistent across all studied scenarios.

Observing the 5D scenario, a constrain on the turbines' C_T values however, shows that there is a trade-off on achieved AEP, resulting in a 36.27% and 56.68% loss in AEP, respectively, by the constrained cases (PSO_{CT} and GA_{CT}) compared to their unconstrained counterparts (PSO and GA). Nonetheless, this trade-off irrespective of its magnitude, may be tolerated considering the high level of adherence to turbine $C_T(\bar{U})$ magnitudes that are achievable plant-wide.

It is established that TI levels vary inversely with U_∞ values. This study demonstrated further that this relationship is also independent of the separation distances between turbines in the WP. Results also show that applying constraints on turbines' C_T values during power maximisation does not significantly affect TI-levels, as no apparent differences are seen between the constrained and unconstrained cases. In addition, the study was also able to show that power maximisation with or without constraining turbine C_T values generally increases WP TI levels most especially in tightly spaced scenarios. The consequence of this is a possible increase in turbine fatigue loads.

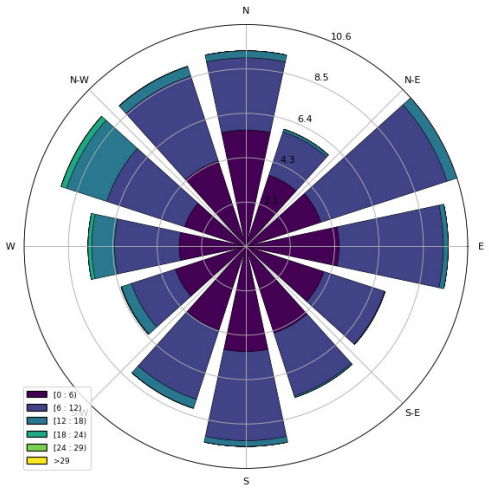

FIGURE 16. Twelve-bin wind rose for WM10 Butterworth at 60 m above ground level.

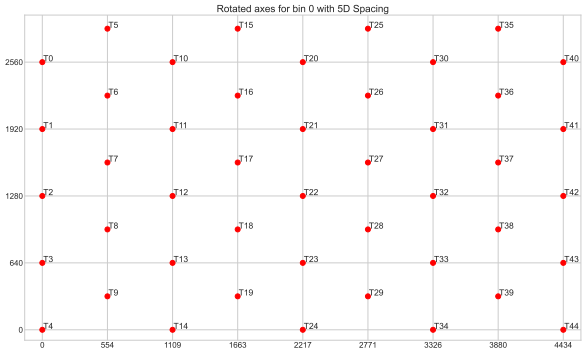

FIGURE 17. WP array at 5D T-2-T distance, Bin 0.

Generally, T-2-T separation distances were shown in the study to have contrasting relationships with turbine C_T values and TI levels, positively correlated with turbine C_T values but negatively correlated with TI levels. For a WP with a hexagonal lattice deployment which has been shown to produce determinate T-2-T distances plant-wide in any considered direction), this relationship could be exploited to obtain a WP system where both turbines' C_T values and TI levels are maintained within acceptable limits.

APPENDIX A
SITE DETAILS

The studied site is located in Butterworth, in the Eastern Cape province of South Africa. The wind data spans a 10-year period between March 2011 to February 2012, October 2012 to December 2014, and January 2016 - May 2022, and can be obtained via a free online registration at WASA-1 Project. The windrose for the period is depicted in Fig. 16.

APPENDIX B
WIND PLANT DEPLOYMENT DETAILS

See Figures 17–19.

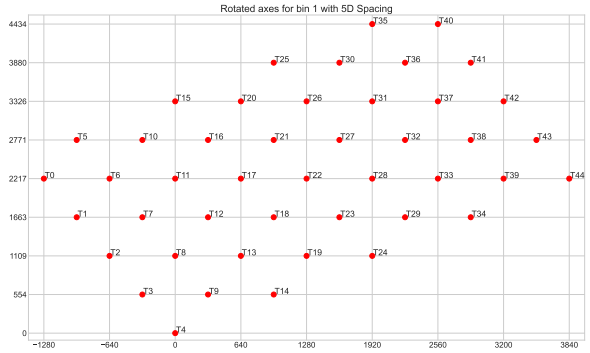

FIGURE 18. WP array at 5D T-2-T distance, Bin 1.

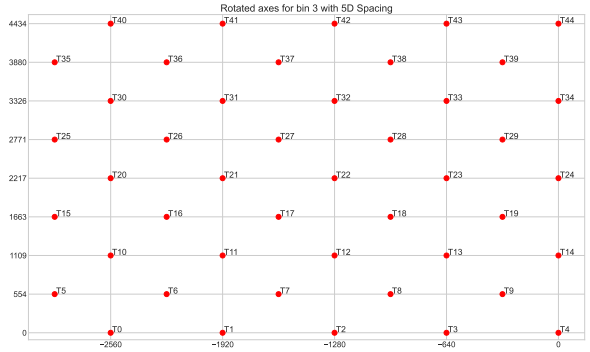

FIGURE 19. WP array at 5D T-2-T distance, Bin 3.

ACKNOWLEDGMENT

Special thanks go to Stephen Ekwe, Sunday Oladejo, and Lateef Akinyemi for their technical engagements regarding the optimization algorithms and mathematical formulations. The author Mfon O. Charles also acknowledge the all-round support of the Power Systems Research Group and the Center for Broadband Networks, Department of Electrical Engineering, University of Cape Town. Computations were performed using facilities provided by the University of Cape Town's ICTS High Performance Computing team: hpc.uct.ac.za.

REFERENCES

[1] A. Niayifar and F. Porté-Agel, "Analytical modeling of wind farms: A new approach for power prediction," *Energies*, vol. 9, no. 9, p. 741, Sep. 2016.
[2] P. Fleming, P. Gebraad, J.-W. van Wingerden, S. Lee, M. Churchfield, A. Scholbrock, J. Michalakes, K. Johnson, and P. Moriarty, "SOWFA super-controller: A high-fidelity tool for evaluating wind plant control approaches," Nat. Renew. Energy Lab. (NREL), Golden, CO, USA, Tech. Rep. NREL/CP-5000-57175, 2013.
[3] G.-W. Qian and T. Ishihara, "A new analytical wake model for yawed wind turbines," *Energies*, vol. 11, no. 3, p. 665, Mar. 2018.
[4] J. Park and K. H. Law, "Layout optimization for maximizing wind farm power production using sequential convex programming," *Appl. Energy*, vol. 151, pp. 320–334, Aug. 2015.
[5] N. Gionfra, G. Sandou, H. Siguerdidjane, D. Faille, and P. Loevenbruck, "Wind farm distributed PSO-based control for constrained power generation maximization," *Renew. Energy*, vol. 133, pp. 103–117, Apr. 2019.
[6] J. J. Barradas-Berglind and R. Wisniewski, "Wind farm axial-induction factor optimization for power maximization and load alleviation," in *Proc. Eur. Control Conf. (ECC)*, Jun. 2016, pp. 891–896.
[7] M. Charles, D. T. Oyedokun, and M. Dlodlo, "Annual energy production maximisation effects on turbine thrust coefficient and turbulence intensity," in *Proc. IEEE AFRICON*, Oct. 2023, pp. 1–6.

[8] A. Brand and J. Wagenaar, "A quasi-steady wind farm flow model in the context of distributed control of the wind farm," in *Proc. Eur. Wind Energy Conf. Exhib. (EWEC)*, Warsaw, Poland, Apr. 2010, p. 31.
[9] P. Gebraad, J. J. Thomas, A. Ning, P. Fleming, and K. Dykes, "Maximization of the annual energy production of wind power plants by optimization of layout and yaw-based wake control," *Wind Energy*, vol. 20, no. 1, pp. 97–107, Jan. 2017.
[10] P. A. Fleming, A. Ning, P. M. O. Gebraad, and K. Dykes, "Wind plant system engineering through optimization of layout and yaw control," *Wind Energy*, vol. 19, no. 2, pp. 329–344, Feb. 2016.
[11] N. Guo, M. Zhang, B. Li, and Y. Cheng, "Influence of atmospheric stability on wind farm layout optimization based on an improved Gaussian wake model," *J. Wind Eng. Ind. Aerodynamics*, vol. 211, Apr. 2021, Art. no. 104548.
[12] R. H. Thuillier and U. O. Lappe, "Wind and temperature profile characteristics from observations on a 1400 ft tower," *J. Appl. Meteorol.*, vol. 3, no. 3, pp. 299–306, Jun. 1964. [Online]. Available: https://journals.ametsoc.org/view/journals/apme/3/3/1520-0450_1964_003_0299_watpcf_2_0_co_2.xml
[13] G. Gualtieri, "Comparative analysis and improvement of grid-based wind farm layout optimization," *Energy Convers. Manage.*, vol. 208, Mar. 2020, Art. no. 112593.
[14] F. Liu, X. Ju, N. Wang, L. Wang, and W.-J. Lee, "Wind farm macro-siting optimization with insightful bi-criteria identification and relocation mechanism in genetic algorithm," *Energy Convers. Manage.*, vol. 217, Aug. 2020, Art. no. 112964.
[15] M. F. Howland, S. K. Lele, and J. O. Dabiri, "Wind farm power optimization through wake steering," *Proc. Nat. Acad. Sci. USA*, vol. 116, no. 29, pp. 14495–14500, Jul. 2019.
[16] P. A. Fleming, P. M. O. Gebraad, S. Lee, J.-W. van Wingerden, K. Johnson, M. Churchfield, J. Michalakes, P. Spalart, and P. Moriarty, "Evaluating techniques for redirecting turbine wakes using SOWFA," *Renew. Energy*, vol. 70, pp. 211–218, Oct. 2014.
[17] P. M. Gebraad, F. Teeuwisse, J. van Wingerden, P. A. Fleming, S. Ruben, J. Marden, and L. Pao, "Wind plant power optimization through yaw control using a parametric model for wake effects—A CFD simulation study," *Wind Energy*, vol. 19, no. 1, pp. 95–114, Jan. 2016.
[18] G.-W. Qian and T. Ishihara, "Wind farm power maximization through wake steering with a new multiple wake model for prediction of turbulence intensity," *Energy*, vol. 220, Apr. 2021, Art. no. 119680.
[19] J. Cao, X. Gao, X. Shen, H. Sun, and Y. Ju, "Wake-based wind turbine optimisations under yawed conditions," in *Proc. 7th Int. Conf. Environ. Friendly Energies Appl. (EFEA)*, Dec. 2022, pp. 1–5.
[20] E. Bossanyi, "Combining induction control and wake steering for wind farm energy and fatigue loads optimisation," *J. Phys., Conf. Ser.*, vol. 1037, Jun. 2018, Art. no. 032011.
[21] M. Charles, D. T. O. Oyedokun, and M. Dlodlo, "Power maximization and turbulence intensity management through axial induction-based optimization and efficient static turbine deployment," *Energies*, vol. 14, no. 16, p. 4943, Aug. 2021.
[22] S. Frandsen, "Turbulence and turbulence generated loading in wind turbine clusters," Risø DTU Nat. Lab. Sustain. Energy, Roskilde, Denmark, Risø Rep. R-1188, 2007.
[23] P. Argyle, S. Watson, C. Montavon, I. Jones, and M. Smith, "Modelling turbulence intensity within a large offshore wind farm," *Wind Energy*, vol. 21, no. 12, pp. 1329–1343, Dec. 2018.
[24] S. Bauer and L. Matysik. *Gamesa G128-5.0MW*. Accessed: Jul. 12, 2021. [Online]. Available: https://en.wind-turbine-models.com/turbines/767-gamesa-g128-5.0mw
[25] B. Andresen, "Wake behind a wind turbine operating in yaw," M.S. thesis, Institutt for energi-og prosessteknikk, Trondheim, Norway, 2013.
[26] Á. Jiménez, A. Crespo, and E. Migoya, "Application of a LES technique to characterize the wake deflection of a wind turbine in yaw," *Wind Energy*, vol. 13, no. 6, pp. 559–572, Sep. 2010.
[27] J. F. Manwell, J. G. McGowan, and A. L. Rogers, *Wind Energy Explained: Theory, Design and Application*. Hoboken, NJ, USA: Wiley, 2010.
[28] *Wind Turbines—Part 1: Design Requirements*, Standard IEC 61400-1, 3rd ed., European Commission, 2005.
[29] M. K. Heris. (2020). *Practical Genetic Algorithms in Python and MATLAB—Video Tutorial*. Accessed: Jul. 12, 2022. [Online]. Available: https://yarpiz.com/632/ypga191215-practical-genetic-algorithms-in-python-and-MATLAB
[30] M. Heris, "Particle swarm optimization (PSO) in Python," *Yarpiz*, vol. 22, Feb. 2017, pp. 79–87.
[31] S. Tao, Q. Xu, A. Feijóo, G. Zheng, and J. Zhou, "Nonuniform wind farm layout optimization: A state-of-the-art review," *Energy*, vol. 209, Oct. 2020, Art. no. 118339.
[32] M. K. Heris, "Particle swarm optimization (PSO) in Python," Yarpiz, 2017. [Online]. Available: https://yarpiz.com/463/ypea127-pso-in-python

MFON O. CHARLES (Member, IEEE) received the B.Sc. degree from the University of Calabar, Nigeria, the first M.Sc. degree in information and communications engineering from the University of Leicester, U.K, and the second M.Sc. degree in engineering physics from the University of Calabar, Nigeria. He is currently pursuing the Ph.D. degree in electrical engineering with the University of Cape Town, South Africa. He is a Lecturer I with the Department of Physics, University of Calabar, Nigeria. He is passionate about clean energy and seeks to explore communication topologies for future smart farms that will reduce capital costs through efficient turbine deployments and consequently reduce inter-turbine cabling, reduce O & M costs by conserving communication bandwidth and reducing both extreme and fatigue loads, and finally increase revenue through improved power generation. He was a recipient of the Third Best Paper Award from the Annual Southern Africa Telecommunication Networks and Applications Conference (SATNAC), in November 2021.

DAVID T. O. OYEDOKUN (Senior Member, IEEE) received the B.Sc., M.Sc., and Ph.D. degrees in electrical engineering from the University of Cape Town (UCT), South Africa, in 2007, 2010, and 2015 respectively. He was a Postdoctoral Reearcher with the South African National Space Agency (SANSA). He is currently an Associate Professor with the Department of Electrical Engineering, UCT, specializing in power system stability, geomagnetically induced currents, renewable energy, and power delivery optimization. He has published several peer-reviewed research articles and a book chapter. He was a recipient of the IEEE MGA GOLD Achievement Award, in 2011. He is currently the IEEE South Africa Section Chair. He has served on several IEEE committees.

MQHELE E. DLODLO (Life Member, IEEE) received the B.S. and B.S. E.E. degrees in mathematics and engineering management from the Geneva College, Beaver Falls, PA, USA, the M.S.E.E. degree from Kansas State University, Manhattan, KS, USA, and the Ph.D. degree from TU Delft, The Netherlands. He is currently a Professor and the Vice-Chancellor of the National University of Science and Technology (NUST), Zimbabwe (nust.ac.zw). He is also an Emeritus Associate Professor/a member of the Communications Research Group (CRG), Telkom Centre of Excellence (CoE), for broadband networks and applications, and co-supervising the Ph.D. students with the Department of Electrical Engineering, University of Cape Town (uct.ac.za). Since 1983, he has been a Wireless Communication Systems Researcher, a Fulbright Senior Scholar Alumnus, FZweIE, and FAS in higher education, prior plant engineering technician.